Virtual Spherical Modes for AoA Estimation With Small Subwavelength Antennas

Linta Antony, *Graduate Student Member, IEEE*, Abel Zandamela, *Member, IEEE*, Nicola Marchetti, *Senior Member, IEEE*, and Adam Narbudowicz, *Senior Member, IEEE*

***Abstract*—Phased arrays are pivotal for determining the angle of arrival (AoA) of signals. However, they are impractical for size-constrained and weight-constrained platforms. Recently developed spherical modes (SM) multiport antennas offer a compact beamforming solution due to their ability to generate multiple radiating modes within a confined volume. This work exploits this methodology by introducing a sparse sensing (SS) technique to generate additional virtual SM, increasing the degrees of freedom (DoF) of AoA detection. It is demonstrated that SS with MUltiple SIgnal Classification (MUSIC) and estimation of signal parameters via rotational invariance technique algorithms can identify up to six uncorrelated sources with a five-port SM beamforming antenna, resulting in the number of simultaneously detected sources being greater than the number of ports used. The technique allows for increased accuracy, computational efficiency, and DoF for AoA estimation, highlighting its potential for Internet of Things applications.**

***Index Terms*—Angle of arrival (AoA) estimation, Estimation of Signal Parameters via Rotational Invariance Technique (ESPRIT), multiple-input–multiple-output (MIMO), MUltiple SIgnal Classification (MUSIC), small Internet of Things (IoT) platforms, sparse sensing (SS), spherical modes (SM).**

I. Introduction

ANGLE of arrival (AoA) estimation determines the transmitter's position by analyzing incoming signal angles on multiple antennas without clock synchronization [1]. Although larger antenna apertures enhance angular accuracy, reducing antenna size while maintaining accuracy poses a significant challenge. Moreover, simultaneous detection of multiple signals usually requires larger antenna arrays, as algorithms like MUltiple SIgnal Classification (MUSIC) typically need $N+1$ antennas to separate N signals [2]. However, the trend toward miniaturization challenges the feasibility of large arrays, prompting the need for innovative solutions to achieve precise AoA estimation in compact devices [3].

Manuscript received 17 July 2024; accepted 3 August 2024. Date of publication 9 August 2024; date of current version 4 December 2024. This work was supported by Microsoft and SFI through CONNECT Centre through the Science Foundation Ireland (SFI) and Digitising Biodiversity Project, through a Trinity College Dublin Kinsella Challenge-Based E3 Award, and Nature+CONNECT under Grant 13/RC/2077_P2. *(Corresponding author: Adam Narbudowicz.)*

Linta Antony and Nicola Marchetti are with Trinity College Dublin, D02 XH97 Dublin, Ireland.

Abel Zandamela was with Trinity College Dublin, D02 XH97 Dublin, Ireland. He is now with Quadsat, 5270 Odense, Denmark.

Adam Narbudowicz is with Tyndall National Institute, D08 WV88 Dublin, Ireland, and also with the Wroclaw University of Science and Technology, 50-370 Wroclaw, Poland (e-mail: adam.narbudowicz@tyndall.ie).

Digital Object Identifier 10.1109/LAWP.2024.3441513

Recent advancements in AoA estimation are based on the theory of characteristic modes and its application to multiport antennas. Functionally, a multimode multiple-input–multiple-output (MIMO) antenna behaves similarly to an antenna array [4]. However, classical array design incorporates just a single physical radiator that is interspaced at uniform or nonuniform distance, and the phase difference between the elements is explored to realize the AoA estimation. On the other hand, multimode MIMO antennas explore a single physical radiator to simultaneously excite different radiating modes [5], [6], [7], which makes them compact when compared to linear arrays while exciting the same number of modes, or using the same number of ports [8]. Moreover, miniaturization is realized with good coupling characteristics because of the orthogonality of the modes.

Much research on multiport antennas has focused on their MIMO communication potential [9], [10], with only a few studies delving into AoA estimation. In [11], the discussion revolves around MIMO antennas utilized for AoA estimation, showcasing a compact design achieved by activating orthogonal characteristic modes within a single element. Meanwhile, Grundmann et al. [12] proposed weight coefficients for the characteristic modes of cubic structures. Despite these innovations, size constraints continue to challenge antenna design. However, a recent study [13] demonstrates that compact multimode antennas can achieve or surpass the performance of larger, traditional arrays with an equivalent number of RF transceivers, offering effective localization solutions for small Internet of Things (IoT) devices. These studies show that in multimode antennas, resolution is tied to the number of effectively excited modes. The degrees of freedom (DoF), indicating the antenna's capacity to resolve multiple signals, is capped at $M-1$, where M is the number of excited spherical modes (SM). Thus, enhancing resolution necessitates generating more modes. However, stimulating numerous modes within a confined space can compromise bandwidth and increase losses.

This letter introduces for the first time the concept of virtual SM, synthesized by exploiting the second-order statistics of received signals and tapping into the sparse phase difference between the modes. This principle significantly increases the number of simultaneously distinguishable signals beyond the limit of $M-1$.

II. Spherical Modes Beamforming (SMB)

The SMB principle was first proposed in [14]. The method is based on the simultaneous excitation of numerous

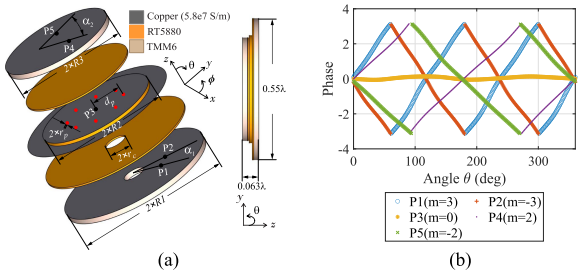

Fig. 1. SMB. (a) Exploded-view of the proposed antenna. Dimensions (in mm): feed points—P1 = P2 = 16.5, P3 = 0, P4 = P5 = 9.5, $R_1 = 36.9$, $R_2 = 28$, $R_3 = 26.9$, and $r_c = 5.25$, and radius of the vias (shown in red dots)—$r_p = 0.25$, $d_p = 15$, $\alpha_1 = 225°$, $\alpha_2 = 30°$. (b) Phase patterns as reported in [14].

omnidirectional SM. By exploiting the different phase distributions of their radiation patterns, constructive interference can be generated toward the chosen direction(s) to realize continuous beamforming across the entire azimuthal plane.

Unlike classical arrays that radiate a single mode and create the necessary phase variations through interelement spacing, the SMB antenna design employs collocated radiators, offering a substantial size reduction without compromising accuracy. The required phase variations are achieved by rotating the electric field in opposite directions around the antenna's perimeter, based on the number of phase turns for each radiated mode. This principle, therefore, provides sufficiently distinct phase variations for AoA estimation. Fig. 1(a) shows an SMB antenna discussed in [14]. It is fed using five ports to excite the desired five orthogonal omnidirectional SM with a maximum dimension of 0.55λ. Fig. 1(b) demonstrates the phase distribution of the radiation patterns generated by five modes with indexes: $m = \{-3, -2, 0, +2, +3\}$. $m = \pm 3$ excites the modes with triple-phase variations. $m = \pm 2$ excites the modes with dual-phase variations. Finally, $m = 0$ excites the fundamental mode with a constant phase. Mode order $m = \pm 1$ with an omnidirectional pattern is not feasible due to physical limitations. This is because, in the $m = \pm 1$ mode, the main radiation is produced toward the poles, with right-hand circular polarization being radiated toward one pole, and left-hand circular polarization being radiated toward the other pole. This produces a bidirectional radiation, with main beams oriented in different plane than the other modes used.

III. Signal Model for SMB Antenna

Consider an SMB antenna receiving D narrowband signals S_d impinging from directions $\{\theta_d,\ d = 1, 2, \ldots, D\}$, each with power σ_d^2.

Let m be a set of integers specifying the phase variations of the antenna's radiation pattern in the azimuthal plane. The radiation pattern from the kth port can be approximated by the function [15]

$$\mathbf{e}_k(\theta) = e^{-jm_k\theta} \tag{1}$$

where m_k is the kth element of set m. For a convention, m can be arranged in ascending order, i.e., the first entry in m is the min(m), and the last entry is the max(m). This configuration aligns with experimentally validated antennas [8], [14], and the phase patterns are depicted in Fig. 1(b). The received signals are represented by the column vector $\mathbf{X}_m$ and expressed as [15]

$$\mathbf{X}_m = \sum_{d=1}^{D} S_d \mathbf{E}_m(\theta_d) + \mathbf{n}_m \tag{2}$$

where $\mathbf{E}_m(\theta)$ is the antenna response vector, a column vector with elements $e^{-jm_k\theta}$ for each $m_k \in m$, and $\mathbf{n}_m$ is the additive white Gaussian noise vector with covariance $E[\mathbf{n}_m\mathbf{n}_m^H] = \sigma^2\mathbf{I}$. The antenna and source signals are assumed to be coplanar in the horizontal plane, i.e., $\phi = 90°$.

IV. Sparse Sensing (SS) Using SM

SS techniques, utilizing second-order statistics, have been explored in various sparse arrays with different sensor arrangements [16], [17], [18], [19]. In this context, we are adapting these SS techniques for SMB antennas. To apply the principle of SS to SMB antennas, we transform the received data into its second-order statistics by computing the covariance matrix of the received data $\mathbf{X}_m$. The covariance matrix of $\mathbf{X}_m$ is defined as [16]

$$\mathbf{R}_{X_m}(\theta) = E[\mathbf{X}_m\mathbf{X}_m^H] = \sum_{d=1}^{D} \sigma_d^2 \mathbf{E}_m(\theta_d)\mathbf{E}_m^H(\theta_d) + \sigma^2\mathbf{I} \tag{3}$$

where $\mathbf{E}_m(\theta_d)\mathbf{E}_m^H(\theta_d)$ results in a matrix with entries $e^{j\theta(m_i - m_j)}$ for $m_i, m_j \in m$, i.e., phase differences.

The vectorized form of $\mathbf{E}_m(\theta_d)\mathbf{E}_m^H(\theta_d)$ is an antenna response vector defined by $\{m_i - m_j | m_i, m_j \in m\}$. The elements in $\mathbf{R}_{X_m}$ represent pairwise differences of signals received at each antenna port. Since the phase differences between these ports are sparse, these pairwise differences generate new, unique samples. Thus, for k ports, calculating all pairwise differences effectively simulates new samples as if received by a virtual port with new modes. The vectorized covariance matrix vec($\mathbf{R}_{X_m}$) can be represented as follows [16]:

$$\mathbf{X}_{m_{\text{diff}}} = (\mathbf{E}_m^* \odot \mathbf{E}_m)\mathbf{P} + \sigma^2\tilde{\mathbf{e}} \tag{4}$$

where $(\cdot)^*$ denotes conjugation, $\odot$ represents the Khatri–Rao product, $\mathbf{P}$ is a column vector of signal powers, and $\tilde{\mathbf{e}}$ is a vector comprised of unit vectors $\mathbf{i}_k$, each with a "1" in the position corresponding to the difference element in m_{diff}. Consequently, the noise vector in m_{diff} is deterministically characterized as $\sigma^2\tilde{\mathbf{e}}$. By vectorizing $\mathbf{R}_{X_m}$, it can be regarded as an equivalent received signal from a virtual multiport antenna with a corresponding antenna response matrix $(E_m^* \odot E_m)$.

Definition 1: (Sparse modes difference set): The sparse modes difference set can be defined as the set of all possible pairwise differences between the elements in m. The set $m_{\text{diff}} = \{m_i - m_j | m_i, m_j \in m\}$ encapsulates all pairwise phase differences.

Definition 2: (Redundancy function): Let w be a function defined on the set m_{diff} such that for any element $d \in m_{\text{diff}}$, $w(d)$ denotes the number of occurrences of d in the set m_{diff}. Then, $\mathbf{X}_{m_{\text{diff}}}$ can be defined as

$$\mathbf{X}_{m_{\text{diff}}}|_d = \frac{1}{|w(d)|} \sum_{(m_i, m_j) \in w(d)} \mathbf{R}_{\mathbf{x}_m}|_{m_i, m_j}$$

for all $d \in m_{\text{diff}}$. It is desirable to have sufficiently small values for a $w(d)$. As d occurs more than once in m_{diff}, then it implies a drop in the DoF of m_{diff}. For an SMB antenna with M SM, the redundancy function evaluated at zero equals M, i.e., $w(0) = M$. For any nonzero element d in m_{diff}, the redundancy function satisfies $1 \leq w(d) \leq M-1$. The function is symmetric, so $w(d) = w(-d)$ for all $d \in m_{\text{diff}}$. The total weight sum for all nonzero elements in m_{diff} is given by $\sum_{d \in m_{\text{diff}}, d \neq \vec{0}} w(d) = M(M-1)$. Considering these properties, the maximum DoF for m_{diff} is $M(M-1)+1$. Therefore, by strategically optimizing the modes within a compact-sized SMB antenna, the system can detect more sources simultaneously than the number of excited SM without necessitating bandwidth reduction or incurring additional losses.

The covariance-derived $\mathbf{X}_{m_{\text{diff}}}$ embodies inherent data correlations, causing $\mathbf{X}_{m_{\text{diff}}}$ to behave like a single snapshot. The rank of the covariance matrix calculated from this equivalent virtual SMB antenna's received signal is one. To enable AoA estimation methods, such as MUSIC [20], and estimation of signal parameters (ESPRIT) [21] to detect multiple sources, a high-rank matrix is necessary. ESPRIT, in particular, capitalizes on the rotational invariance property by utilizing identical sensor pairs, known as doublets. While the deployment of ESPRIT in uniformly spaced antenna arrays has proven to be straightforward and efficient, adapting it to the signal matrix $\mathbf{X}_m$ of multiport antennas presents distinct challenges [15]. This stems from the antenna manifold $\mathbf{E}_m$ within $\mathbf{X}_m$, which lacks the Vandermonde structure prerequisite for ESPRIT. However, when considering the differential domain signal $\mathbf{X}_{m_{\text{diff}}}$, the restructured manifold $(\mathbf{E}_m^* \odot \mathbf{E}_m)$ aligns with Vandermonde's form, rendering it compatible with the ESPRIT framework.

Nonetheless, the covariance-derived $\mathbf{X}_{m_{\text{diff}}}$ embodies inherent data correlation, complicating the application of ESPRIT and MUSIC, which presuppose uncorrelated signal sources for accurate AoA estimation. To effectively address the inherent data correlations within $\mathbf{X}_{m_{\text{diff}}}$, it is essential to decorrelate the data. Hermitian symmetry is equivalent to $\mathbf{x}_{m_{\text{diff}}}|_d = \mathbf{x}_{m_{\text{diff}}}|_{-d}^*$ for $d \in m_{\text{diff}}$. Which is based on these properties: $|w(d)| = |w(-d)|$ for $d \in m_{\text{diff}}$. Exploiting this symmetry is a key to constructing a positive semidefinite Toeplitz matrix $\mathbf{R}$ [18], to ensure appropriate matrix rank (required for high-resolution AoA estimation algorithms to perform effectively). The matrix $\mathbf{R}$ is constructed by reshaping $\mathbf{X}_{m_{\text{diff}}}$ as follows:

$$\mathbf{R} = \begin{bmatrix} [\mathbf{X}_{m_{\text{diff}}}]_L & [\mathbf{X}_{m_{\text{diff}}}]_{L-1} & \cdots & [\mathbf{X}_{m_{\text{diff}}}]_1 \\ [\mathbf{X}_{m_{\text{diff}}}]_{L+1} & [\mathbf{X}_{m_{\text{diff}}}]_L & \cdots & [\mathbf{X}_{m_{\text{diff}}}]_2 \\ \vdots & \vdots & \ddots & \vdots \\ [\mathbf{X}_{m_{\text{diff}}}]_{2L-1} & [\mathbf{X}_{m_{\text{diff}}}]_{2L-2} & \cdots & [\mathbf{X}_{m_{\text{diff}}}]_L \end{bmatrix} \quad (5)$$

where $L = (|\mathbf{m}_{\text{diff}}|+1)/2$, with $|\mathbf{m}_{\text{diff}}|$ representing the cardinality of the set $\mathbf{m}_{\text{diff}}$. Applying high-resolution algorithms, such as MUSIC and ESPRIT, to $\mathbf{R}$ enables the resolution of $L-1$ uncorrelated sources. With the proposed sparse-based approach, for an SMB antenna with M SM, the maximum number of identifiable sources $L-1$ can be constrained as $M-1 < L-1 \leq (M(M-1))/2$.

Fig. 2(a) shows the elements and their redundancy in m_{diff} for an SMB antenna with $m = \{-3, -2, 0, +2, +3\}$, comprising 13 elements: $m_{\text{diff}} = \{-6, -5, -4, -3, -2, -1, 0, +1, +2, +3, +4, +5, +6\}$. These new modes correspond to distinct antenna response vectors, and the cardinality $|m_{\text{diff}}| - 1$ indicates the maximum number of detectable simultaneous signals. However, by reshaping $\mathbf{X}_{m_{\text{diff}}}$ into a Toeplitz matrix, it acts as the covariance matrix of the received data from an antenna configured with seven distinct modes, with phase variances $V = \{0, +1, +2, +3, +4, +5, +6\}$. Fig. 2(b) shows the phase patterns corresponding to these modes, facilitating the simultaneous detection of six uncorrelated signals using a five-port antenna with $m = \{-3, -2, 0, +2, +3\}$.

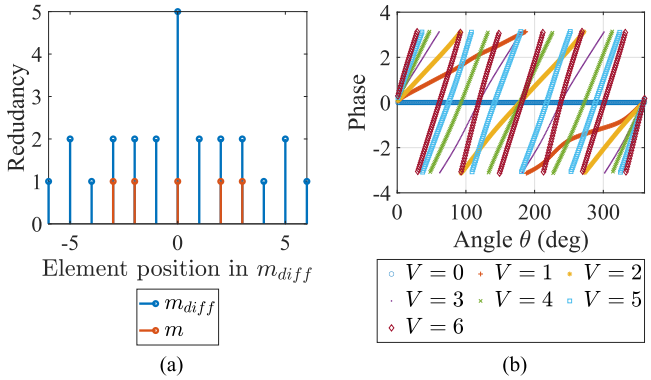

Fig. 2. (a) Phase difference set m_{diff} of virtual SM. (b) Phase patterns of virtual SM.

A. Complexity analysis of the proposed method

Using a sparse-based MUSIC or ESPRIT approach, an SMB antenna with M SM can detect up to $L-1$ sources. With state-of-art MUSIC, detecting $L-1$ sources requires L modes, $O(S|L|^2)$ operations for covariance matrix calculation for S snapshots, $O(|L|^3)$ for eigenvalue decomposition, and $O(Q|L|^2)$ for angle grid search, where Q is the number of possible angles used in the grid search, totaling $O(S|L|^2 + |L|^3 + Q|L|^2)$. For ESPRIT, the angle search is replaced with AoA estimation from the rotational invariance matrix, which only requires $O((L-1)^3)$ operations. Therefore, the total operations for ESPRIT is $O(S|L|^2 + |L|^3 + (L-1)^3)$. Additional steps for AoA estimation using sparse-based MUSIC and ESPRIT include the construction of $\mathbf{x}_{m_{\text{diff}}}$ and $\mathbf{R}$. Since $\mathbf{x}_{m_{\text{diff}}}$ is constructed from the covariance matrix $\mathbf{R}_{\mathbf{X}_m}$ and the calculation of $\mathbf{R}$ involves the rearrangement of $\mathbf{x}_{m_{\text{diff}}}$, these additional steps do not require any new multiplier operations. Thus, this proposed approach does not increase complexity.

V. Results

The proposed methodology was simulated using exemplary radiation patterns of antenna reported in [14]. This was studied for two cases: using ideal radiation patterns with perfect phase dependencies and full-wave simulated radiation patterns (including phase imperfections and coupling effects) obtained from CST Microwave Studio.

All AoA estimations were executed using MATLAB version: R2022a (64-bit), Operating System: Windows 10 Pro

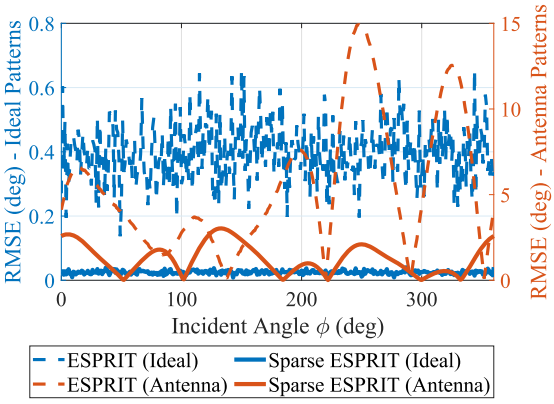

Fig. 3. RMSE versus angle for ESPRIT with and without sparse approach on ideal patterns and antenna patterns (SNR= 15 dB and $N = 100$).

(64-bit) with 11th Gen Intel Core i5-1135G7 at 2.40GHz processor and 8 GB of RAM.

The accuracy of the estimates is quantified using the root-mean-square error (RMSE), which is formulated as follows [22]:

$$\text{RMSE} = \sqrt{\frac{1}{DN}\sum_{d=1}^{D}\sum_{i=1}^{N}(\theta_d - \hat{\theta}_{d,i})^2} \tag{6}$$

where N is the number of Monte Carlo simulations. The term $\hat{\theta}_{d,i}$ denotes the estimated value of the AoA θ_d in the ith Monte Carlo simulation. For this study, N is set to 100. The signal-to-noise ratio (SNR) is set to 15 dB.

Fig. 3 illustrates the accuracy differences between ESPRIT applied with and without a sparse approach on ideal radiation patterns and the radiation patterns generated by antenna [14]. ESPRIT typically requires pairs of identical sensors, known as doublets, for effective AoA estimation. In an ESPRIT implementation without a sparse approach, doublets are configured using available phase patterns: $m1$ and $m3$ from the first doublet and $m4$ and $m2$ from the second. Applying a sparse approach introduces seven virtual modes with uniform phase variations, which simplifies ESPRIT's application and allows the use of six doublets instead of two. This adaptation results in a significantly lower RMSE with the sparse approach compared to the ESPRIT without the sparse approach. The behavior of RMSE for the antenna-generated patterns, both with and without the sparse approach, is due to discrepancies in some angles of the radiation pattern compared to the ideally expected radiation patterns. Nonetheless, it can be seen that the error due to these phase imperfections is less for the sparse-based approach to antenna-generated patterns.

For the five-port antenna employed in this study, $L = 7$. Consequently, both MUSIC and ESPRIT can detect up to six uncorrelated sources. Fig. 4 depicts the detection of six uncorrelated sources from the directions 50°, 100°, 150°, 200°, 250°, and 300° using the SS methodology. Both algorithms reveal six distinct peaks at the specified angles. Furthermore, as observed in Fig. 5, for ideal phase patterns, it is evident that as SNR increases, RMSE decreases for both MUSIC and ESPRIT. However, for antenna-generated patterns, due to discrepancies in some angles of the phase patterns compared

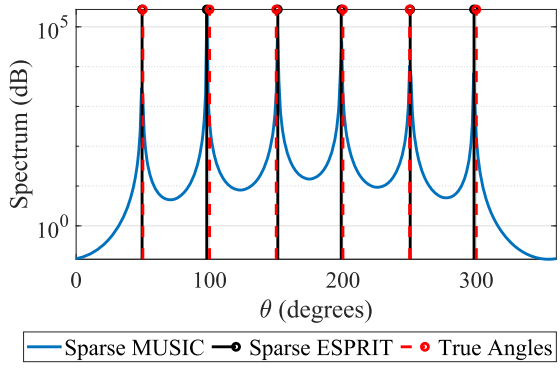

Fig. 4. Multiple source estimation using sparse based MUSIC and ESPRIT with five ports (SNR= 15 dB and $N = 100$).

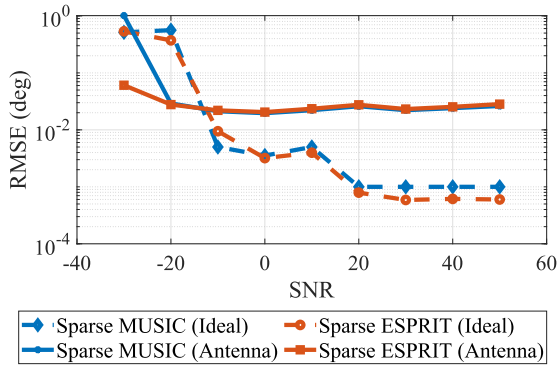

Fig. 5. RMSE versus SNR for SS-based MUSIC and ESPRIT on ideal and antenna generated phase patterns of five port SMB antenna for two sources $\in (0°, 360°)$.

to the theoretically expected radiation patterns as per (1), the accuracy of MUSIC and ESPRIT does not improve with SNR. This is a limitation of the method as it is prone to phase imperfections in the radiation pattern compared to the ideal radiation pattern. These phase imperfections can contribute more error than Gaussian noise to the performance of the proposed algorithm. This is a limitation of this approach; however, based on Fig. 3, it can be seen that errors due to phase imperfections are considerably less for the proposed sparse approach than for the nonsparse approach on SMB antenna. Nevertheless, the accuracy of both MUSIC and ESPRIT is comparable in both cases. ESPRIT improves computational efficiency over MUSIC by eliminating the necessity for grid-based angle finding. Therefore, for applications requiring AoA estimation, the SS-based ESPRIT methods on an SMB antenna emerge as an optimal choice, ensuring compactness, expanded DOF, and computational efficiency.

VI. Conclusion

This work demonstrates SS on SMB antennas, leveraging different spatial phase distributions between these modes by utilizing second-order statistics. It is noteworthy that the SS with ESPRIT can identify up to six uncorrelated sources with five inputs. With computational advantages over methods, such as MUSIC, SS with ESPRIT on SMB antennas emerges as a good solution for compact IoT systems.

REFERENCES

[1] F. Zafari, A. Gkelias, and K. K. Leung, "A survey of indoor localization systems and technologies," *IEEE Commun. Surveys Tuts.*, vol. 21, no. 3, pp. 2568–2599, 3rd Quart. 2019.

[2] T. E. Tuncer and B. Friedlander, *Classical and Modern Direction-of-Arrival Estimation*. San Francisco, CA, USA: Academic, 2009.

[3] Y. Li et al., "Toward location-enabled IoT (LE-IoT): IoT positioning techniques, error sources, and error mitigation," *IEEE Internet Things J.*, vol. 8, no. 6, pp. 4035–4062, Mar. 2021.

[4] R. Martens and D. Manteuffel, "Systematic design method of a mobile multiple antenna system using the theory of characteristic modes," *Microw., Antennas Propag.*, vol. 8, no. 12, pp. 887–893, 2014.

[5] F. A. Dicandia, S. Genovesi, and A. Monorchio, "Advantageous exploitation of characteristic modes analysis for the design of 3-D null-scanning antennas," *IEEE Trans. Antennas Propag.*, vol. 65, no. 8, pp. 3924–3934, Aug. 2017.

[6] N. Peitzmeier, T. Hahn, and D. Manteuffel, "Systematic design of multimode antennas for MIMO applications by leveraging symmetry," *IEEE Trans. Antennas Propag.*, vol. 70, no. 1, pp. 145–155, Jan. 2022.

[7] L. Grundmann and D. Manteuffel, "Evaluation method and design guidance for direction-finding antenna systems," *IEEE Trans. Antennas Propag.*, vol. 71, no. 9, pp. 7146–7157, Sep. 2023.

[8] A. Zandamela, A. Chiumento, N. Marchetti, and A. Narbudowicz, "Angle of arrival estimation via small IoT devices: Miniaturized arrays vs. MIMO antennas," *IEEE Internet Things Mag.*, vol. 5, no. 2, pp. 146–152, Jun. 2022.

[9] M. Burtowy, M. Rzymowski, and L. Kulas, "Low-profile ESPAR antenna for RSS-based DoA estimation in IoT applications," *IEEE Access*, vol. 7, pp. 17403–17411, 2019.

[10] C. Y. Kataria, G. X. Gao, and J. T. Bernhard, "Design of a compact hemispiral GPS antenna with direction finding capabilities," *IEEE Trans. Antennas Propag.*, vol. 67, no. 5, pp. 2878–2885, May 2019.

[11] R. Pöhlmann, S. A. Almasri, S. Zhang, T. Jost, A. Dammann, and P. A. Hoeher, "On the potential of multi-mode antennas for direction-of-arrival estimation," *IEEE Trans. Antennas Propag.*, vol. 67, no. 5, pp. 3374–3386, May 2019.

[12] L. Grundmann, N. Peitzmeier, and D. Manteuffel, "Investigation of direction of arrival estimation using characteristic modes," in *Proc. IEEE 15th Eur. Conf. Antennas Propag.*, 2021, pp. 1–5.

[13] A. Zandamela, A. Chiumento, N. Marchetti, M. J. Ammann, and A. Narbudowicz, "Exploiting multimode antennas for MIMO and AoA estimation in size-constrained IoT devices," *IEEE Sens. Lett.*, vol. 7, no. 3, Mar. 2023, Art. no. 5500904.

[14] A. Zandamela, N. Marchetti, M. J. Ammann, and A. Narbudowicz, "Spherical modes driven directional modulation with a compact MIMO antenna," *IEEE Antennas Wireless Propag. Lett.*, vol. 22, no. 3, pp. 477–481, Mar. 2023.

[15] L. Antony, A. Zandamela, N. Marchetti, and A. Narbudowicz, "Angle of arrival estimation methods using spherical-modes-driven multiport antennas," in *2024. Eur. Conf. Antennas Propag.*, 2024, pp. 1–5.

[16] P. Chevalier, L. Albera, A. Ferréol, and P. Comon, "On the virtual array concept for higher order array processing," *IEEE Trans. Signal Process.*, vol. 53, no. 4, pp. 1254–1271, Apr. 2005.

[17] P. Pal and P. P. Vaidyanathan, "Nested arrays: A novel approach to array processing with enhanced degrees of freedom," *IEEE Trans. Signal Process.*, vol. 58, no. 8, pp. 4167–4181, Aug. 2010.

[18] C.-L. Liu and P. Vaidyanathan, "Remarks on the spatial smoothing step in coarray MUSIC," *IEEE Signal Process. Lett.*, vol. 22, no. 9, pp. 1438–1442, Sep. 2015.

[19] D. G. Chachlakis and P. P. Markopoulos, "Structured autocorrelation matrix estimation for coprime arrays," *Signal Process.*, vol. 183, 2021, Art. no. 107987.

[20] R. Schmidt, "Multiple emitter location and signal parameter estimation," *IEEE Trans. Antennas Propag.*, vol. AP-34, no. 3, pp. 276–280, Mar. 1986.

[21] R. Roy and T. Kailath, "ESPRIT-estimation of signal parameters via rotational invariance techniques," *IEEE Trans. Acoust., Speech, Signal Process.*, vol. 37, no. 7, pp. 984–995, Jul. 1989.

[22] R. J. Hyndman and A. B. Koehler, "Another look at measures of forecast accuracy," *Int. J. Forecasting*, vol. 22, no. 4, pp. 679–688, 2006.